NON-INVASIVE ACTIVE THERMOMETRY WITH A MICROWAVE TOMOGRAPHIC SCANNER IN HYPERTHERMIA TREATMENTS.

J. J. Mallorquí, A. Broquetas, L. Jofre, A. Cardama
Grup Antenes-Microones-Radar, Dept. Teoria del Senyal i Comunicacions.
ETSETB, Universitat Politècnica de Catalunya.
P.O. Box 30002, 08080 Barcelona, SPAIN

ABSTRACT

In this work the active microwave tomographic imaging of tissue temperature changes induced in deep hyperthermia treatments is studied. The thermal images would allow to monitor and optimize the treatment, increasing its efficacy and avoiding the heating of healthy tissues. As some hyperthermia systems are based on a cylindrical geometry, it is possible to integrate a microwave imaging array in the same structure, providing a non-invasive tool for the monitoring and control. The application of this technique to deep hyperthermia treatments is investigated by numerical simulations and experimentally on two phantoms of thorax and pelvis, using a prototype for microwave tomography recently developed [Jofre et al, 1990].

INTRODUCTION

Forming images of the human body using ionizing radiation has been a part of the diagnostic process in medicine for many years. More recently, other probing radiations, notably ultrasound, have provided successful diagnostic images. Tomography is now in widespread use in the clinic with ionizing radiations (X-ray,isotopes) and with nuclear magnetic resonance imaging. In the past few years, other probing radiations have been considered for tomography, including ultrasound [Mueller et al 1979][Duchene and Tabara, 1985], very low-frequency electromagnetic fields in electrical impedance tomography [Barber et al., 1983] and microwave.

Hyperthermia has shown considerable promise for the adjuvant treatment of cancer, but it is essential to heat the tumor region with a high degree of precision. Ideally the temperature throughout the volume of both the tumor and surrounding normal tissue would be known so one could determine the degree of uniformity of treatment to the tumor and also estimate the extent of possible damage to the normal tissue. When radio-frequency energy is used to induce hyperthermia, much of the heating may occur outside the region intended for treatment. Aberrant heating is especially significant when frequencies below 1 GHz are used to treat deep-seated tumors. Such undesired heating is likely to go undetected during a treatment session since there are practical limits on the number of temperature probes that may be used. In practice temperature probes are used for measurements at only a few intracavity or interstitial locations [Conway and Anderson, 1986]. Thus it will be useful to develop a non-invasive method to obtain a thermal map of a body under hyperthermia treatment, that allows improve hyperthermia treatments.

Microwave active imaging is a promising non-invasive method for thermography imaging, thus biological tissues have a high dependence of dielectric constant with temperature changes. Active microwave imaging consists of illuminating the body to be imaged with a low-power coherent microwave field and measuring the field scattered by the body. The measured data can be processed using specialized diffraction inverse algorithms to give information on the complex dielectric permittivity of the scattering body.

SYSTEM DESCRIPTION

A cylindrical tomographic microwave system working at 2.45 GHz has been recently developed. The scanner consists of a 64 element circular array with a useful diameter of 20 cm. Although the array is in fact circular, the name cylindrical is used because each antenna is assumed to produce an almost cylindrical wave on the illuminated region. Antennas are electronically scanned, alternately as sources and receivers, to give a complete scan of the object with no mechanical movement. The incident power is less than 0.1 mW/cm^2 at the object and require a coupling medium (in this case water) between object and the source/receiver [Broquetas et al, 1991].

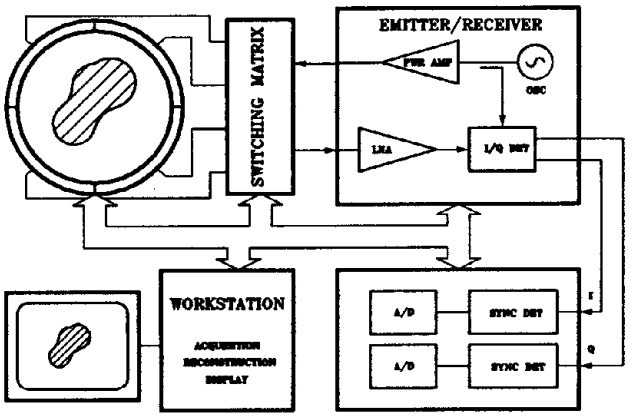

Fig. 1 Block diagram of the prototype system.

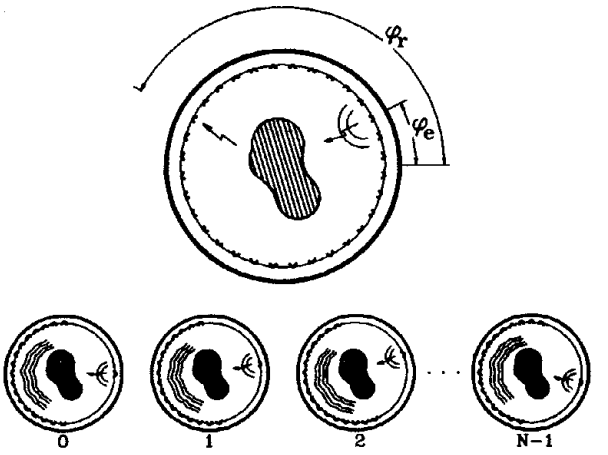

Fig. 2 Measurement procedure in a cylindrical system; with the angular coordinates of the emitter and receiver antennas in operation. The object is illuminated sequentially with the elements of the array (views); for each view the scattered fields are measured.

IMAGING ALGORITHM

Unlike X rays, microwave radiation has a wavelength comparable to the size of object; thus refraction and diffraction cannot be neglected and diffraction imaging algorithms must be used. In a cylindrical array the field produced by each element will be approximately a cylindrical wave emerging from the antenna if the field energy is assumed to be confined to the thickness of the array. For each emitter the scattered field will be measured on other elements of the array, yielding a matrix $E_s(\varphi_r, \varphi_e)$, where φ_r is the angular position of the receiver element and φ_e the angular position of the emitter, as shown in Fig. 2.

Using an electric field polarized axially and neglecting depolarization effects in the body, we can use an approximate scalar representation of currents and electric field [Slaney and Kak, 1985]. Conventional algorithms are based on linear geometries of measurement and make use of first-order approximations, which means that the body is assumed to perturbate slightly the incident field. Illuminating the body with a plane wave, the plane wave angular spectrum of the scattered field contains the spectrum of the dielectric contrast of the object along circles of radius k_0 (the wavenumber of the field in the embedding reference medium). The dielectric contrast $C(\vec{r})$ is the relative difference between the complex permittivity of each point of the body $\varepsilon(\vec{r})$ and the reference permittivity ε_0 corresponding to the embedding medium:

$$C(\vec{r}) = 1 - \varepsilon(\vec{r})/\varepsilon_0 \qquad (1)$$

In our case the geometry of measurement is cylindrical and a similar algorithm can be obtained based on Hankel transforms; however this algorithm is difficult to implement on a digital computer and very inefficient because of the large number of Bessel functions involved.

A much more efficient algorithm can be obtained by using a synthetic approach to form plane waves as a combination of cylindrical waves. Due the linearity of the scattering and using the reciprocity theorem the Fourier bidimensional spectrum of $C(\vec{r})$

$$\tilde{C}(\vec{\eta}) = \mathcal{F}\{C(\vec{r})\} = \int_{-\infty}^{\infty} C(\vec{r}) e^{-j\vec{\eta}\cdot\vec{r}} d\vec{r} \qquad (2)$$

can be related to the scattered fields [Rius et al., 1987]. The spectral domain is obtained on circular arcs of radius k_0 with coordinates $\vec{\eta} = k_0(\hat{\theta} - \hat{\theta}_0)$, where $\hat{\theta}_0$ and $\hat{\theta}$ are unit vectors in the directions of illuminating and

scattered plane waves:

$$\tilde{C}[k_0(\hat{\theta}-\hat{\theta}_0)]=\frac{j}{\omega\varepsilon_0}\int_0^{2\pi}\int_0^{2\pi}E_s(\varphi_r,\varphi_e)J_a(\varphi_r;-\hat{\theta})$$

$$\cdot J_a(\varphi_e;\hat{\theta}_0)R^2 d\varphi_r d\varphi_e \qquad (3)$$

where R is the radius of the array. Equation (3) is formally a double convolution of the measured scattered fields E_s with the currents on the array J_a that would produce a plane wave illumination, The convolution can be efficiently calculated using FFT techniques as a double product in the spectral domain between the Fourier series of E_s and J as described in [Rius et al., 1987]. The image obtained by inverse bidimensional Fourier transform once $\tilde{C}[k_0(\hat{\theta}-\hat{\theta}_0)]$ has been mapped on a rectangular grid by linear interpolation in a way similar to that in linear algorithms. The reconstruction time is 30 s on a HP9000-320 workstation [Rius et al., 1987].

Unfortunately, most biological bodies causes the breakdown of the Born approximation due to their high contrast characteristics and large size in terms of wavelengths. It has been found both numerically and experimentally that some biological bodies with sections of a few wavelengths can be reconstructed, revealing qualitatively their internal structures. When the size is larger, it is possible to get useful differential reconstructions showing dielectric changes.

In thermography, the image is reconstructed from the difference between the fields scattered by the reference and the heated body. Ideally the image should represent the dielectric changes induced by heating. Unfortunately there are terms of error and the image is qualitative and does not reconstruct the original permittivity values. However, in this case the image still supplies information on the situation of thermal changes induced. In preliminary experiments to estimate the temperature sensitivity of the system a rubber tube 0.05 mm thick and 3 cm internal diameter was placed off center in the water tank; heated water was pumped through the tube and a temperature resolution of the system of 0.5 °C was found [Jofre et al., 1990]. In the present work the thermal sensitivity of high contrast large biological bodies is investigated.

All images in the paper represent the object profile, defined as $C(\vec{r})=1-\varepsilon(\vec{r})/\varepsilon_0$.

NUMERICAL SIMULATION

The frequency is a compromise between spatial resolution, with a theoretical limit of one half of the wavelength, and attenuation. The spatial resolution improves with frequency but, due to the high water content of biological tissues, the operating frequency is limited by the maximum attenuation that can be tolerated in the field measurements. The behaviour of the imaging algorithm depends on the electrical size of the object, this is an additional factor that must be considered in the choice of the optimum frequency. The useful imaging diameter depends on the number of antennas and the wavelength of the external medium.

$$D=\frac{2N\lambda_0}{4\pi} \qquad (4)$$

The frequencies to study are 434 MHz, 700 MHz and 915 MHz allowing a reasonable resolution and level of attenuation. In all cases 64 antennas are enough to reconstruct a human trunk, with an average width of 38 cm. A simulated tomographic scanner based on a 60 cm diameter array with 64 antennas has been adopted.

Numerical models of sections of thorax and pelvis have been defined with a discretization step of 0.1 λ for each frequency. Fig. 3 shows the numerical model and phantoms of anatomic sections [Karitké and Sick, 1988]. Table 1 shows the permittivity of tissues taken form [Stuchly, 1980][Iskander, 1978].

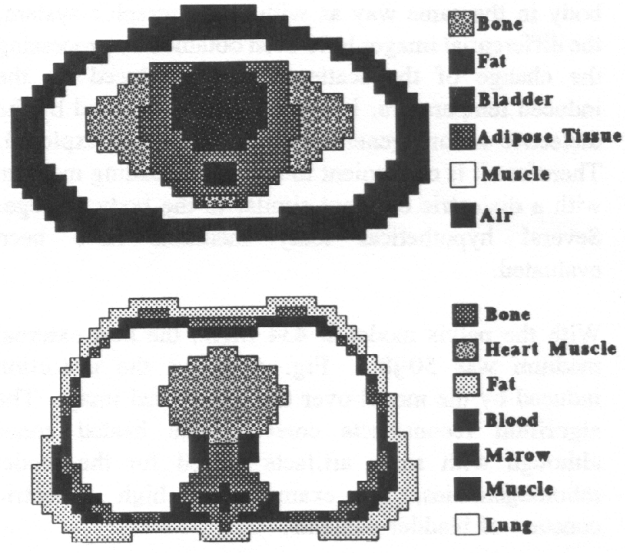

Fig. 3 Numerical and phantom models of thorax and pelvis.

TISSUE PERMITTIVITY			
Tissue	**434 MHz**	**700 MHz**	**915 MHz**
Fat	5.5-j3.3	5.5-j2.0	4.6-j1.1
Muscle	53-j41.4	53-j30.8	54-j23.6
Heart Muscle	56-j38.5	55-j28.2	55-j21.6
Bone	8.5-j1.3	8.5-j0.8	8-j1
Bladder	50-j16.5	50-j10.2	-
Lung	36-j25.2	34-j19.5	35-j14.3
Marrow	5.5-j1.2	5.5-j0.8	5.5-j0.6
Adipose Tissue	20-j9	20-j8.1	-
Blood	63-j49.7	62-j30.2	63-j24.5
Thermal Sensitivity	$100(\Delta\varepsilon'/\varepsilon')/^{\circ}C$	$100(\Delta\varepsilon''/\varepsilon'')/^{\circ}C$	
Fat	1.2	4.6	
Muscle	-0.2	1.3	
Lung	-0.2	1.5	

Table 1. Permittivity and thermal sensitivity of human tissues

Using the Conjugate Gradient Method (CGM-MM) to calculate the scattered fields by the reference and heated body in the same way as with a tomographic system, the differential images have been obtained by processing the change of the scattered field produced by the induced temperature. Image artifacts are caused by the dielectric inhomogeneities of the materials explored. Therefore it is convenient to use an embedding medium with a dielectric constant similar to the body average. Several hypothetical lossy mediums have been evaluated.

With the pelvis model at 434 MHz, the best external medium was 50-j8.5. Fig. 4 shows the distortion induced by the model over the differential image. The algorithm reconstructs correctly the heated zones although with some artifacts caused for the model inhomogeneities, for example the high dielectric constant of bladder contents.

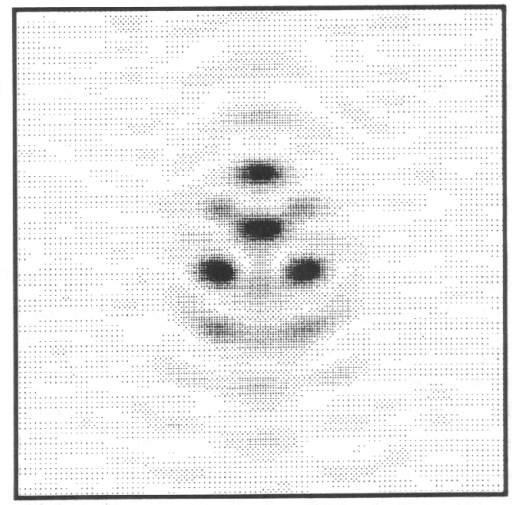

Fig. 4 Pelvis model at 434 MHz with 2 heated zones (5° C) in internal adipose tissue.

Fig. 5 shows 4 heated zones in the pelvis model at 434 MHz, the effect of mismatching between losses of body and external medium causes a radial variation in the image, resulting in lower thermal sensitivity at internal zones than external.

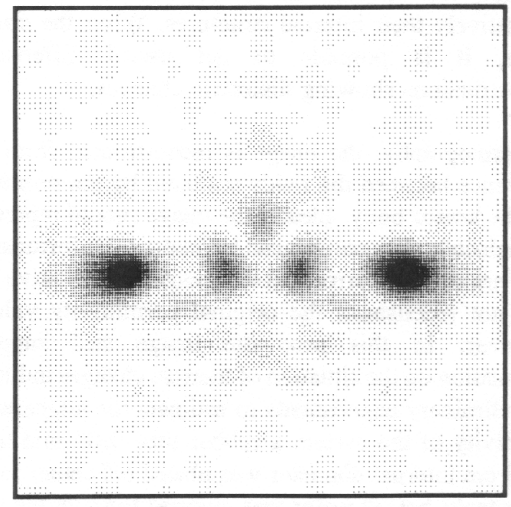

Fig. 5 Pelvis model at 434 MHz with 4 heated zones (5°C), 2 internal and 2 external, and a bladder contents equal to external media.

In the higher frequencies, the distortion introduced by the body on the incident field increases resulting in more artifacts. Thus, we can conclude that the optimal frequency for pelvis monitoring with a first order

algorithm is 434 MHz.

A similar study has been performed on a thorax model. The higher homogeneity of this body allows to reconstruct thermal changes up to 900 MHz with low artifact levels. Fig. 6 shows 6 heated zones with temperatures increases of 5 °C, 3 ° C and 1 °C; the first one is perfectly visible, the second one have a minor level and the third one is visible, but it may be confused with other erroneous spots.

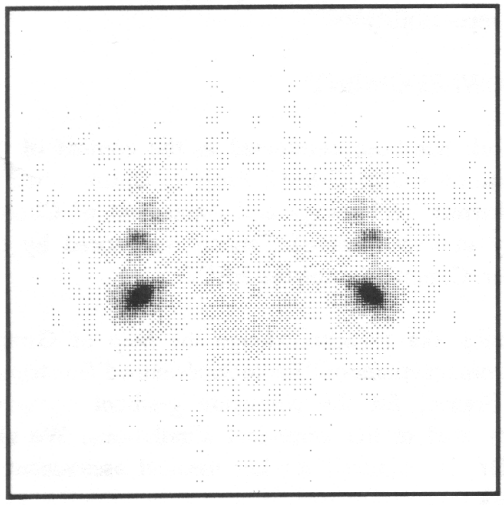

Fig. 6 Thorax model at 700 MHz with six heated zones.

EXPERIMENTAL STUDY

From the results obtained by numerical simulations, phantoms have been constructed in order to simulate at study frequencies the electrical properties of thorax and pelvis. The experimental prototype works at 2.45 GHz using water as outer medium. In order to reproduce the electrical size and contrast of the numerical simulations, the complex permittivity and dimensions of the phantoms have been calculated using the electromagnetic scaling expressions [Sinclair, 1948] at Table 2.

The phantoms are simplified versions of the numerical models consisting of a plaster outer shell to simulate skin and external fat, including gels simulating muscle, bladder and lung [Kato et al., 1986] and plaster simulating bone. Several thin plastic tubes were added to simulate internal heating by chemical dielectric alterations.

Due to the prototype sensitivity limitations and the high attenuation of biological tissues, only large dielectric changes were reconstructed. Fig. 7 shows a pelvis phantom at 434 MHz with a focalized change in bladder of 14+j0.2 in permittivity. This was the minor change detected in this model.

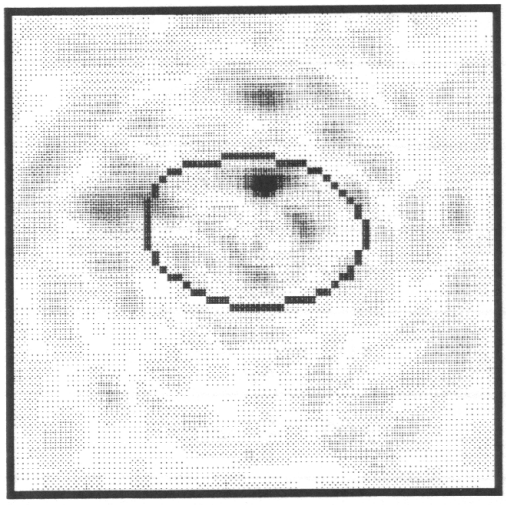

Fig. 7 Pelvis phantom at 434 MHz with a focalized change in bladder.

In thorax phantoms better results have been obtained. Fig. 8 shows a phantom at 700 MHz with a increment in permittivity of 5+j15. Also this case was the minor change detected in the model.

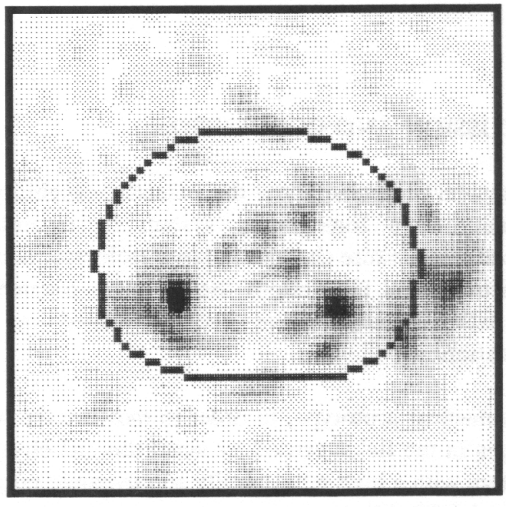

Fig. 8 Thorax phantom at 700 MHz with 2 heated zones.

Real System A	Simulated System A'
$\vec{r} = p\vec{r}'$	
$t = \gamma t'$	$\omega = \frac{1}{\gamma}\omega'$
$\vec{E}(\vec{r},t) = \alpha \vec{E}'(\vec{r}',t')$	
$\vec{H}(\vec{r},t) = \beta \vec{H}'(\vec{r}',t')$	
$\sigma(\vec{r}) = \frac{\beta}{\alpha p}\sigma'(\vec{r}')$	
$\varepsilon(\vec{r}) = \frac{\gamma\beta}{\alpha p}\varepsilon'(\vec{r}')$	
$\mu(\vec{r}) = \frac{\alpha\gamma}{\beta p}\mu'(\vec{r}')$	
If magnetic materials not scaled ... $\mu(\vec{r}) = \mu'(\vec{r}')$	
$t = \gamma t'$	$\vec{r} = \frac{\alpha\gamma}{\beta}\vec{r}'$
$\sigma(\vec{r}) = \frac{\gamma}{p^2}\sigma'(\vec{r}')$	$\varepsilon(\vec{r}) = \frac{\beta^2}{\alpha^2}\varepsilon'(\vec{r}')$

Table 2. Relations obtained from Maxwell's Equations.

DISCUSSION AND CONCLUSION

The results presented show the potential capability of the microwave tomography system to reconstruct induced temperature changes in large biological bodies. From numerical simulations the optimum frequencies and external media have been estimated in this application.

For a medical prototype, in order to measure the weak changes in the fields caused by small thermal changes, a system with a high repeatability and dynamic range is required (100 dB).

The algorithm is capable to reconstruct thermal changes in homogeneous bodies, but in the case of large inhomogeneities, erroneous spots appear in the final image. This is due to the limitations caused by the Born approximation algorithm. New algorithms based in iterative techniques are in study; and first results obtained are considerably better than using Born approximation. The problem with this new type of algorithms is the large computational time and large amount of memory necessary to obtain good results. The big advantage of presented imaging algorithm is the computational speed, for example in an HP-Apollo 700/RX station measured data could be processed in real time.

Research will continue to improve reconstruction algorithms, increase sensitivity (dynamic range) and system repeatability.

ACKNOWLEDGMENT

This work has been conducted in the context of the collaboration COMAC-BME Project "Optimization of Hyperthermia Technology and Assesment of Clinical Efficacy in Treatment of Cancer" sponsored by the European Commission of the EEC.

We would like to acknowledge the help of Groupe d'Electromagnetisme of l'Ecole Supérieure d'Electricité, Paris, France, for the conjugate gradient computer program used in the numerical simulations. We also thank Dr. H. Almirall for her medical assessment in this work.

REFERENCES

[Barber et al, 1983] D.C. Barber, B.H. Brown, I.L. Freeston, "Imaging Spatial Distributions of Resistivity Using Applied Potential Tomography", *Electron. Lett.*, Vol 19, No 22, pp. 933-934, 1983.

[Broquetas et al, 1991] A. Broquetas, J. Romeu, J.M. Rius, A.R. Elías-Fusté, A. Cardama, L. Jofre, "Cylindrical Geometry: A Further Step in Active Microwave Tomography", *IEEE Trans. on MTT*, Vol. 39, No 5, pp. 836-844, May 1991.

[Conway and Anderson, 1986] J. Conway, A.P. Anderson, "Electromagnetic Techniques in Hyperthermia", *Clin. Phys. Physical Meas.*, Vol. 7, No 4, pp 287-318, 1986.

[Duchene and Tabara, 1985] B. Duchene, W. Tabbara, "Tomographie ultrasonore par diffraction", *Rev. Phys. Appl.*, No 6, pp 299-304, June 1985.

[Iskander, 1978] M.F. Iskander, *Radiofrequency Radiation Dosimetry Handbook*, 2nd ed., Dep. of Electrical Eng. & Bioeng., University of Utah, pp 58-61, May 1978.

[Jofre et al, 1990] L. Jofre, M.S. Hawley, A. Broquetas, E. de los Reyes, M. Ferrando and A. Elías, "Medical imaging with a Microwave Tomographic Scanner", *IEEE-BME*, Vol. 37, No 3, pp. 303-312, March 1990.

[Karitké and Sick, 1988] Karitké/Sick, *Atlas of Sectional Human Anatomy*, Urban and Scharzenberg, 2nd ed.,1988.

[Kato et al, 1986] H. Kato et al., "An Agar Phantom for Hyperthermia", *Medical Physics*, Vol 13, No 3, 1986.

[Mueller et al, 1979] R.K. Mueller, M. Kaveh, G. Wade, "Reconstructive Tomography and Applications to Ultrasonics", *Proc. IEEE*, Vol 67, pp. 567-587, April 1979.

[Rius et al, 1987] J.M. Rius, M. Ferrando, L. Jofre, A. Broquetas, "Microwave Tomography: An Algorithm for Cylindrical Geometries", *Electron. Lett.*, Vol 23, No 11, pp. 564-565, 1987.

[Sinclair, 1948] G. Sinclair, "Theory of Models of Electromagnetic Systems", *Proceedings of the IRE*, pp 1364-1370, Nov. 1948.

[Slaney and Kak, 1985] M. Slaney, A.C. Kak, "Imaging with Diffraction Tomography", Pardue University, School of Elect. Eng., Tech. Rep. TR-EE 85-5, 1985.

[Stuchly, 1980] M.A. Stuchtly, S.S. Stuchtly, "Dielectric Properties of Biological Substances Tabulated", *Journal of Microwave Power*, No 15, 1980.